Radio Science, Volume 32, Number 5, Pages 1777–1784, September–October 1997

Scattering by grooves of arbitrary profile on cylindrical surfaces

Jean-Fu Kiang
Department of Electrical Engineering, National Chung-Hsing University, Taichung, Taiwan

Abstract. A generalized mode-matching method is developed to study the scattering properties of conducting cylinders with periodic grooves of arbitrary cross section. Reflection matrices are derived to reduce the number of unknowns. This method is illustrated by studying three types of periodic grooves with dielectric filling on a cylindrical surface. Radar cross sections by an incident TE wave are obtained, and the effects of frequency, groove profile, groove depth, and filling permittivity are analyzed.

1. Introduction

Scattering by planar periodical structures has been studied extensively with either one-dimensional profiles [*Peng et al.*, 1975; *Zaki and Neureuther*, 1971] or two-dimensional profiles [*Jin and Volakis*, 1993]. Floquet modes are incorporated to transform the original problem to that of a unit cell, which is then solved by using a mode-matching method or a finite element scheme [*Jin and Volakis*, 1993].

The scattering by single or multiple grooves (cavities) on a ground plane has been studied as canonical problems. *Asvestas and Kleinman* [1994] derived a formulation to study the scattering by an indented screen. *Schiavone et al.* [1993] analyzed the scattering of a finite beamwidth incident wave by multiple grooves by using a mode-matching method. Impedance boundary condition has also been used to solve the scattering problem by a dielectric-filled trough [*Goggans and Shumpert*, 1991]. Finite element methods and their variants are suitable to analyze grooves with arbitrary cross section [*Ramahi and Mittra*, 1991].

Similar techniques can be applied to the cylindrical geometries. *Hoppe and Samii* [1994] studied the scattering of plane waves by a dielectric-coated cylinder by using a higher order impedance boundary condition. *Rulf* [1992] analyzed the scattering by sectored cylinders by using a mode-matching method. *Colak et al.* [1993] analyzed the scattering by a cylinder with slots coated by lossy materials.

Scattering by cylinders with noncircular cross section has attracted the interest of many researchers. *Cabayan and Murphy* [1973] applied a perturbation method to study the scattering of a perfectly conducting circular cylinder with slight roughness. *Boag et al.* [1993] used fictitious patch currents to model the scattering by a doubly periodic nonplanar surface. *Sarabandi and Ulaby* [1991] studied the scattering from corrugated stratified dielectric cylinders. The rough bark layer of trees is modeled as multiple grooves and is shown to reduce the radar cross section of the trees.

In this paper a mode-matching method is formulated where the fields in each groove are expanded in terms of the standing wave basis functions. The azimuthally periodic boundary condition is implemented implicitly. The field distribution is determined by matching the tangential field components on the interface between each groove and the outer region. Since the continuity of tangential fields is imposed on multiple surfaces within each groove, the internal resonance issue encountered in typical cavity scattering problems can be avoided, although without proof.

2. Formulation

In Figure 1 we show a perfectly conducting cylinder with periodic grooves on its surface. The grooves can be categorized as wedge, cavity, and crack types according to the curvature of their boundary contour, which can be approximated by a zigzag curve

Paper number 97RS01439.
0048-6604/97/97RS-01439$11.00

consisting of radial segments and concentric arcs. The zigzag curve is defined such that each groove can be divided into N layers with the lower and upper boundaries of layer (ℓ) located at $\rho = a_\ell$ and $\rho = a_{\ell-1}$, respectively. Assuming that there are P grooves on the surface, the angular span of the ℓth layer of the pth groove is $\phi_{p\ell} \le \phi \le \phi_{p\ell} + \theta_\ell$ where $\phi_{p\ell} = (p + 1/2)2\pi/P - \theta_\ell/2$. A plane wave with its magnetic field parallel to the cylinder axis is incident in the direction of $\hat{x}\cos\alpha + \hat{y}\sin\alpha$. Hence the TE_z modes (H polarization) are excited in each groove and in region (0). The H_z and E_ϕ components in the ℓth layer of the pth groove can be expressed as [*Kong*, 1990; *Harrington*, 1993]

$$H_{p\ell z} = \bar{S}^t_{p\ell}(\phi) \cdot \left[\bar{\bar{J}}_\ell(k_\ell\rho)\cdot\bar{\alpha}_{p\ell} + \bar{\bar{H}}^{(1)}_\ell(k_\ell\rho)\cdot\bar{\beta}_{p\ell}\right]$$
$$E_{p\ell\phi} = -i\eta_\ell \bar{S}^t_{p\ell}(\phi) \cdot \left[\bar{\bar{J}}'_\ell(k_\ell\rho)\cdot\bar{\alpha}_{p\ell} + \bar{\bar{H}}^{(1)'}_\ell(k_\ell\rho)\cdot\bar{\beta}_{p\ell}\right] \quad (1)$$

where $\bar{S}_{p\ell}(\phi)$ is a vector consisting of the sinusoidal basis functions; $\bar{\alpha}_{p\ell}$ and $\bar{\beta}_{p\ell}$ are the vectors consisting of the expansion coefficients; and $\bar{\bar{J}}_\ell(k_\ell\rho)$, $\bar{\bar{J}}'_\ell(k_\ell\rho)$, $\bar{\bar{H}}^{(1)}_\ell(k_\ell\rho)$, and $\bar{\bar{H}}^{(1)'}_\ell(k_\ell\rho)$ are diagonal matrices consisting of the Bessel functions or their derivatives. Explicitly,

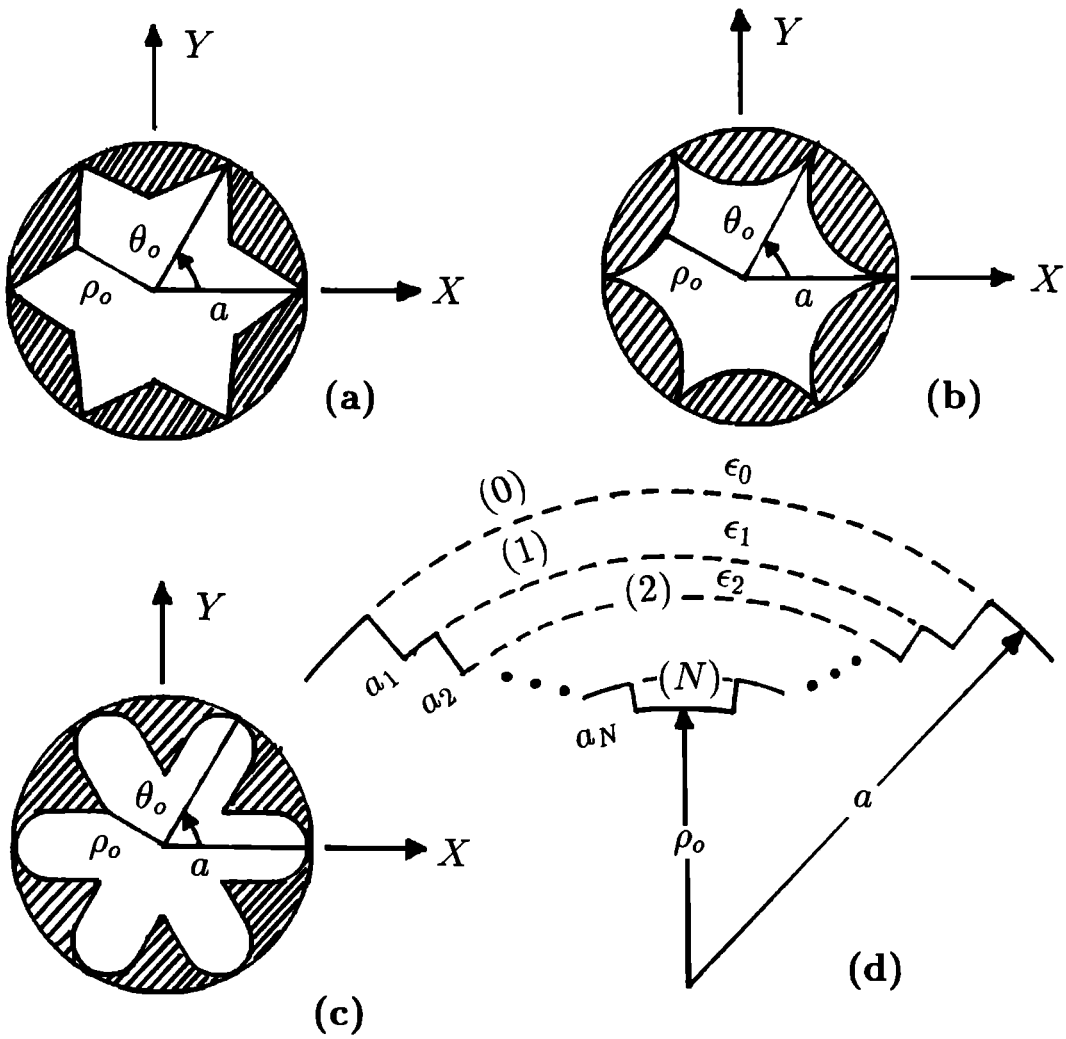

Figure 1. Periodic groove profiles: (a) wedge profile, (b) cavity profile, (c) crack profile, and (d) partitioning of a groove into layers. Hatching represents dielectric filling.

$$\bar{S}_{p\ell}(\phi) = \sqrt{\frac{2}{\theta_\ell}}\left[1/\sqrt{2}, \cos v_\ell(\phi-\phi_{p\ell}), \cos 2v_\ell(\phi-\phi_{p\ell}), \cdots\right]^t$$

$$\bar{\bar{B}}_\ell(k_\ell\rho) = \text{diag.}\left[B_0(k_\ell\rho), B_{v_\ell}(k_\ell\rho), B_{2v_\ell}(k_\ell\rho), \cdots\right], \qquad B = J, H^{(1)}$$

$$\bar{\bar{B}}'_\ell(k_\ell\rho) = \text{diag.}\left[B'_0(k_\ell\rho), B'_{v_\ell}(k_\ell\rho), B'_{2v_\ell}(k_\ell\rho), \cdots\right], \qquad B = J, H^{(1)}$$

with $v_\ell = \pi/\theta_\ell$. Note that the time convention of $e^{-i\omega t}$ is assumed.

Define a reflection matrix $\bar{\bar{R}}_{n\ell}$ at $\rho = a_\ell$ such that

$$\bar{\bar{R}}_{n\ell}\cdot\bar{\bar{J}}'_\ell(k_\ell a_\ell)\cdot\bar{\alpha}_{p\ell} = \bar{\bar{H}}^{(1)'}_\ell(k_\ell a_\ell)\cdot\bar{\beta}_{p\ell}$$

Since $E_{pN\phi} = 0$ at $\rho = a_N$, we have $\bar{\bar{R}}_{nN} = -\bar{\bar{I}}$. At the interface between layers (ℓ) and $(\ell+1)$, we have

$$E_{p\ell\phi} = \begin{cases} E_{p(\ell+1)\phi}, & \phi \in \Omega_{p(\ell+1)} \\ 0, & \text{elsewhere} \end{cases} \tag{2}$$

where $\Omega_{p(\ell+1)} = \{\phi_{p(\ell+1)} \le \phi \le \phi_{p(\ell+1)} + \theta_{\ell+1}\}$, $0 \le p \le P-1$ and $1 \le \ell \le N-1$. Substitute the field expressions in (1) into (2), take the inner product of $\bar{S}_{p\ell}(\phi)$ with the resulting equation, then integrate over $\phi_{p\ell} \le \phi \le \phi_{p\ell} + \theta_\ell$ to have

$$\eta_\ell\left[\bar{\bar{J}}'_\ell(k_\ell a_\ell) + \bar{\bar{H}}^{(1)'}_\ell(k_\ell a_\ell)\cdot\bar{\bar{R}}'_{n\ell}\right]\cdot\bar{\alpha}_{p\ell} = \eta_{\ell+1}\bar{\bar{C}}_{\ell(\ell+1)}\cdot\left[\bar{\bar{J}}'_{\ell+1}(k_{\ell+1}a_\ell) + \bar{\bar{H}}^{(1)'}_{\ell+1}(k_{\ell+1}a_\ell)\cdot\bar{\bar{R}}'_{n(\ell+1)}\right]\cdot\bar{\alpha}_{p(\ell+1)} \tag{3}$$

where $\bar{\bar{C}}_{\ell(\ell+1)} = \langle\bar{S}_{p\ell}(\phi)\bar{S}^t_{p(\ell+1)}(\phi)\rangle$ and

$$\bar{\bar{R}}'_{n\ell} = \left[\bar{\bar{H}}^{(1)'}_\ell(k_\ell a_\ell)\right]^{-1}\cdot\bar{\bar{R}}_{n\ell}\cdot\bar{\bar{J}}'_\ell(k_\ell a_\ell)$$

Similarly, the tangential magnetic field across the interface $\rho = a_\ell$ is continuous; that is,

$$H_{p\ell z} = H_{p(\ell+1)z}, \qquad \phi \in \Omega_{p(\ell+1)} \tag{4}$$

where $0 \le p \le P-1, 1 \le \ell \le N-1$. Substitute the field expressions in (1) into (4), take the inner product of $\bar{S}_{p(\ell+1)}(\phi)$ with the resulting equation, then integrate over $\phi_{p(\ell+1)} \le \phi \le \phi_{p(\ell+1)} + \theta_{\ell+1}$ to have

$$\bar{\bar{C}}_{(\ell+1)\ell}\cdot\left[\bar{\bar{J}}_\ell(k_\ell a_\ell) + \bar{\bar{H}}^{(1)}_\ell(k_\ell a_\ell)\cdot\bar{\bar{R}}'_{n\ell}\right]\cdot\bar{\alpha}_{p\ell} = \left[\bar{\bar{J}}_{\ell+1}(k_{\ell+1}a_\ell) + \bar{\bar{H}}^{(1)}_{\ell+1}(k_{\ell+1}a_\ell)\cdot\bar{\bar{R}}'_{n(\ell+1)}\right]\cdot\bar{\alpha}_{p(\ell+1)} \tag{5}$$

From (3) and (5), a recursive formula for calculating the reflection matrices $\bar{\bar{R}}'_{n\ell}$ is obtained

$$\begin{aligned}\bar{\bar{R}}'_{n\ell} = \Big\{&\bar{\bar{H}}^{(1)'}_\ell(k_\ell a_\ell) - \frac{\eta_{\ell+1}}{\eta_\ell}\bar{\bar{C}}_{\ell(\ell+1)}\\ &\cdot\left[\bar{\bar{J}}'_{\ell+1}(k_{\ell+1}a_\ell) + \bar{\bar{H}}^{(1)'}_{\ell+1}(k_{\ell+1}a_\ell)\cdot\bar{\bar{R}}'_{n(\ell+1)}\right]\\ &\cdot\left[\bar{\bar{J}}_{\ell+1}(k_{\ell+1}a_\ell) + \bar{\bar{H}}^{(1)}_{\ell+1}(k_{\ell+1}a_\ell)\cdot\bar{\bar{R}}'_{n(\ell+1)}\right]^{-1}\\ &\cdot\bar{\bar{C}}_{(\ell+1)\ell}\cdot\bar{\bar{H}}^{(1)}_\ell(k_\ell a_\ell)\Big\}^{-1}\\ \cdot\Big\{&-\bar{\bar{J}}'_\ell(k_\ell a_\ell) + \frac{\eta_{\ell+1}}{\eta_\ell}\bar{\bar{C}}_{\ell(\ell+1)}\\ &\cdot\left[\bar{\bar{J}}'_{\ell+1}(k_{\ell+1}a_\ell) + \bar{\bar{H}}^{(1)'}_{\ell+1}(k_{\ell+1}a_\ell)\cdot\bar{\bar{R}}'_{n(\ell+1)}\right]\\ &\cdot\left[\bar{\bar{J}}_{\ell+1}(k_{\ell+1}a_\ell) + \bar{\bar{H}}^{(1)}_{\ell+1}(k_{\ell+1}a_\ell)\cdot\bar{\bar{R}}'_{n(\ell+1)}\right]^{-1}\\ &\cdot\bar{\bar{C}}_{(\ell+1)\ell}\cdot\bar{\bar{J}}_\ell(k_\ell a_\ell)\Big\}\end{aligned}$$

The fields in region (0) can be expressed as

$$\begin{aligned}E_{0\phi} &= -i\eta_0 H_o\bar{S}^t_0(\phi-\alpha)\cdot\left[\bar{J}'_0(k_o\rho) + \bar{\bar{H}}^{(1)'}_0(k_o\rho)\cdot\bar{\beta}_0\right]\\ H_{0z} &= H_o\bar{S}^t_0(\phi-\alpha)\cdot\left[\bar{J}_0(k_o\rho) + \bar{\bar{H}}^{(1)}_0(k_o\rho)\cdot\bar{\beta}_0\right]\end{aligned} \tag{6}$$

where $\bar{S}_0(\phi-\alpha)$ is a vector containing elements $\{i^n\exp[in(\phi-\alpha)]\}$ with $-\infty < n < \infty$. $\bar{K}_0(k_o\rho)$ is a vector containing elements $\{K_n(k_o\rho)\}$ with $K = J$ or $K = J'$, and $-\infty < n < \infty$. $\bar{\bar{K}}_0(k_o\rho)$ is a diagonal matrix with diagonal elements $\{K_n(k_o\rho)\}$ where $K = H^{(1)}$ or $K = H^{(1)'}$, and $-\infty < n < \infty$. At $\rho = a$ the continuity of tangential electric fields gives

$$E_{0\phi} = \begin{cases} E_{p1\phi}, & \phi \in \Omega_{p1}, 0 \le p \le P-1 \\ 0, & \text{elsewhere} \end{cases} \tag{7}$$

Substitute the field expressions in (1) and (6) into (7), take the inner product of $\bar{S}_0^*(\phi-\alpha)$ with the resulting equation, then integrate over $0 \le \phi \le 2\pi$ to have

$$\eta_0 H_o \left[\bar{J}_0'(k_o a) + \bar{\bar{H}}_0^{(1)'}(k_o a)\cdot\bar{\beta}_0\right] = \sum_{p=0}^{P-1} \bar{\bar{A}}_p \cdot \eta_1 \left[\bar{\bar{J}}_1'(k_1 a) + \bar{\bar{H}}_1^{(1)'}(k_1 a)\cdot\bar{\bar{R}}_{n1}'\right]\cdot\bar{\alpha}_{p1} \quad (8)$$

where

$$\bar{\bar{A}}_p = \frac{1}{2\pi}\int_{\phi_{p1}}^{\phi_{p1}+\theta_1} d\phi \bar{S}_0^*(\phi-\alpha)\bar{S}_{p1}^t(\phi)$$

Similarly, the tangential magnetic field across $\rho = a$ is continuous; that is,

$$H_{0z} = H_{p1z}, \qquad \phi \in \Omega_{p1}, 0 \le p \le P-1 \quad (9)$$

Substitute the field expressions in (1) and (6) into (9), take the inner product of $\bar{S}_{p1}(\phi)$ with the resulting equation, then integrate over $\phi_{p1} \le \phi \le \phi_{p1}+\theta_1$ to have

$$H_o 2\pi \bar{\bar{A}}_p^\dagger \cdot \left[\bar{J}_0(k_o a) + \bar{\bar{H}}_0^{(1)}(k_o a)\cdot\bar{\beta}_0\right] = \left[\bar{\bar{J}}_1(k_1 a) + \bar{\bar{H}}_1^{(1)}(k_1 a)\cdot\bar{\bar{R}}_{n1}'\right]\cdot\bar{\alpha}_{p1} \quad (10)$$

The unknown coefficient vector $\bar{\beta}_0$ can be solved from (8) and (10) to be

$$\bar{\beta}_0 = \left\{\bar{\bar{H}}_0^{(1)'}(k_o a) - 2\pi\frac{\eta_1}{\eta_0}\sum_{p=0}^{P-1}\bar{\bar{A}}_p \cdot \left[\bar{\bar{J}}_1'(k_1 a) + \bar{\bar{H}}_1^{(1)'}(k_1 a)\cdot\bar{\bar{R}}_{n1}'\right]\cdot\left[\bar{\bar{J}}_1(k_1 a) + \bar{\bar{H}}_1^{(1)}(k_1 a)\cdot\bar{\bar{R}}_{n1}'\right]^{-1}\cdot\bar{\bar{A}}_p^\dagger\cdot\bar{\bar{H}}_0^{(1)}(k_o a)\right\}^{-1} \cdot\left\{-\bar{J}_0'(k_o a) + 2\pi\frac{\eta_1}{\eta_0}\sum_{p=0}^{P-1}\bar{\bar{A}}_p \cdot \left[\bar{\bar{J}}_1'(k_1 a) + \bar{\bar{H}}_1^{(1)'}(k_1 a)\cdot\bar{\bar{R}}_{n1}'\right]\cdot\left[\bar{\bar{J}}_1(k_1 a) + \bar{\bar{H}}_1^{(1)}(k_1 a)\cdot\bar{\bar{R}}_{n1}'\right]^{-1}\cdot\bar{\bar{A}}_p^\dagger\cdot\bar{J}_0(k_o a)\right\}$$

If the plane wave is incident upon a smooth circular cylinder with radius a, the reflection coefficients reduce to [Harrington, 1993]

$$\beta_n = -\frac{J_n'(k_o a)}{H_n^{(1)'}(k_o a)} \quad (11)$$

Once the scattering coefficient vector $\bar{\beta}_0$ is obtained, the bistatic radar cross section can be calculated as

$$\sigma_{bi}(\phi,\alpha) = \frac{2\pi\rho|H_{0z}^s|^2}{|H_z^i|^2} = \frac{4}{k_o}\left|\sum_{n=-\infty}^{\infty}\beta_n \exp[in(\phi-\alpha) - i\pi/4]\right|^2$$

where the second equality is obtained by using the conventional stationary phase approximation [Kong, 1990] which accelerates the far field computation and was useful when computers were not as fast as they are today.

3. Results and Discussions

Three types of groove profiles as shown in Figure 1 are considered: wedge, cavity, and crack profile. The groove contour of the wedge profile has an infinite radius of curvature, and that of the cavity (crack) profile has a negative (positive) radius of curvature measured from the cylinder axis. They can be depicted as

$$\text{Wedge profile} \quad \rho\theta = a\theta_o\left(\frac{\rho-\rho_o}{a-\rho_o}\right)$$

$$\text{Cavity profile} \quad \rho\theta = a\theta_o\sqrt{\frac{\rho-\rho_o}{a-\rho_o}}$$

$$\text{Crack profile} \quad \rho\theta = a\theta_o\left(\frac{\rho-\rho_o}{a-\rho_o}\right)^2 \quad (12)$$

where $\rho_o \le \rho \le a$, θ is the azimuthal angle span of the groove at ρ and θ_o is the azimuthal angle span of the groove at $\rho = a$.

Each profile in (12) is approximated by a staircase as shown in Figure 1d. First determine the azimuthal angle span of the outer boundary (θ) in each layer, then determine the radial distance of that outer boundary (ρ) by solving (12) to have

$$\text{Wedge profile} \quad \rho = \frac{a\theta_o\rho_o}{a\theta_o - (a-\rho_o)\theta}$$

$$\text{Cavity profile} \quad \rho = \frac{a(\theta_o/\theta)}{2(a-\rho_o)}\left[a(\theta_o/\theta) - \sqrt{a^2(\theta_o/\theta)^2 - 4\rho_o(a-\rho_o)}\right]$$

$$\text{Crack profile} \quad \rho = \rho_o + \frac{\theta}{\theta_o}\frac{(a-\rho_o)^2}{2a} + (a-\rho_o)\sqrt{\left(\frac{\theta}{\theta_o}\right)^2\frac{(a-\rho_o)^2}{4a^2} + \frac{\theta}{\theta_o}\frac{\rho_o}{a}}$$

By proper choice of the progressive angular spans, only the Bessel and Hankel functions of integer orders are involved, which are less complicated than those with noninteger orders. For example, the angular span of a cylinder with four grooves is chosen to be $\pi/(i+1)$ in region (i).

Figure 2 shows the bistatic radar cross section (RCS) of a cylinder with four wedge grooves. Since no results are available in the literature for cylindrical structures with grooves, we compare the RCS of cylinders carrying very shallow grooves with that of a smooth cylinder using the coefficients in (11). It is observed that the bistatic RCS with $\rho_o = 0.99a$ approaches that of the smooth cylinder as expected. The forward scattering RCS with different ρ_o's are relatively close to one another. When ρ_o is reduced to $0.75a$, the RCS in the directions $55° \le \phi \le 305°$ are significantly different from those of the other three configurations.

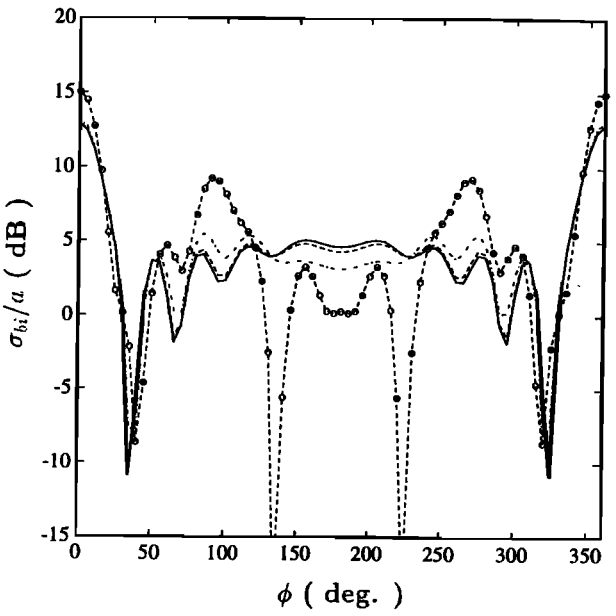

Figure 2. Effects of groove depth on the bistatic radar cross section of a circular cylinder with four wedge grooves, $k_o a = 2\pi$, $\alpha = 0$, and $\epsilon_f = \epsilon_o$: solid line, $\rho_o = a$; dashed line, $\rho_o = 0.99a$; dashed-dotted line, $\rho_o = 0.95a$; dashed line with circles, $\rho_o = 0.75a$.

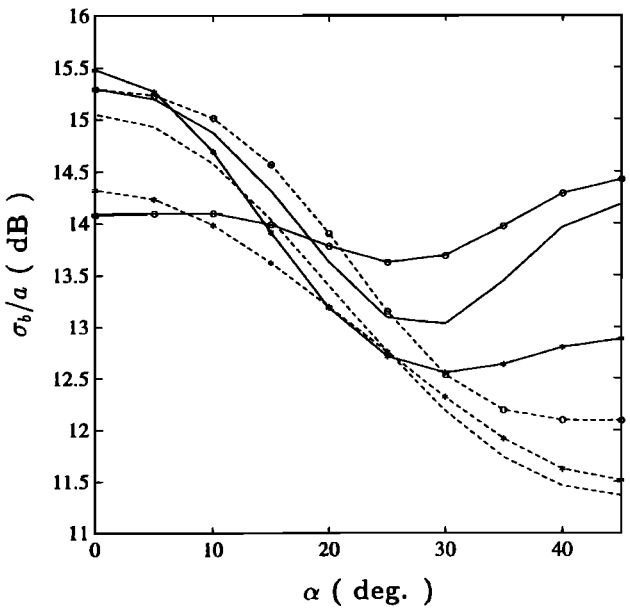

Figure 3. Effects of profile and profile depth on the backscattering cross section of a circular cylinder with four grooves, $k_o a = 2\pi$, and $\epsilon_f = \epsilon_o$: solid line, wedge profile, $\rho_o = 0.5a$; dashed line, wedge profile, $\rho_o = 0.75a$; solid line with circles, cavity profile, $\rho_o = 0.5a$; dashed line with circles, cavity profile, $\rho_o = 0.75a$; solid line with asterisks, crack profile, $\rho_o = 0.5a$; dashed line with asterisks, crack profile, $\rho_o = 0.75a$.

In Figure 3 we show the backscattering RCS of a cylinder with different groove profiles and profile depths. For the wedge profile with $\rho_o = 0.5a$ the RCS decreases from the maximum of 15.30 dB at $\alpha = 0$ to the minimum of 13.03 dB around $\alpha = 30°$ and then increases to 14.19 dB at $\alpha = 45°$. For the concave profile the RCS decreases from 14.08 dB at $\alpha = 0$ to the minimum of 13.63 dB around $\alpha = 25°$, and then increases to the maximum of 14.42 dB at $\alpha = 45°$. For the crack profile the RCS decreases from the maximum of 15.48 dB to the minimum of 12.55 dB around $\alpha = 30°$, and then increases to 12.88 dB at $\alpha = 45°$. The cavity profile has the lowest

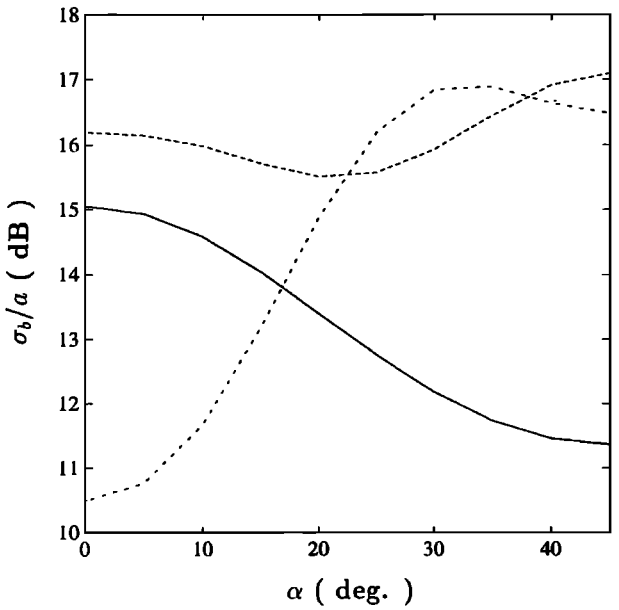

Figure 4. Effects of filling permittivity on the backscattering cross section of a circular cylinder with four wedge grooves, $k_o a = 2\pi$, and $\rho_o = 0.75a$: solid line, $\epsilon_f = \epsilon_o$; dashed line, $\epsilon_f = 2\epsilon_o$; dashed-dotted line, $\epsilon_f = 4\epsilon_o$.

maximum RCS and RCS variation range, while the crack profile has the highest maximum RCS and RCS variation range. At $\rho_o = 0.75a$ the RCS curves of all the three profiles have similar slopes. The cavity profile has the highest maximum RCS, while the crack profile has the lowest maximum RCS; both occur when the incident wave faces the profile hill at $\alpha = 0$.

In Figure 4 we show the effect of filling permittivity on the RCS of a wedge groove. When $\epsilon_f = \epsilon_o$, the RCS decreases with increasing α. When $\epsilon_f = 2\epsilon_o$, the RCS decreases with α within $0 \leq \alpha \leq 20°$, and then increases to the maximum at $\alpha = 45°$. The minimum RCS with $\epsilon_f = 2\epsilon_o$ is even higher than the maximum RCS with $\epsilon_f = \epsilon_o$. As ϵ_f is increased to $4\epsilon_o$, the RCS variation range becomes as wide as 6.39 dB with the maximum occurring around $\alpha = 35°$.

Figure 5 shows the effects of filling permittivity on the RCS of the other two profiles. The RCS curves of the crack profile with $\epsilon_f = \epsilon_o$ and $\epsilon_f = 2\epsilon_o$ look similar to those of the wedge profile. But the RCS variation range of the crack profile with $\epsilon_f = 4\epsilon_o$ is about 2.77 dB, which is less than half of that of the wedge profile. As for the cavity profile with $\epsilon_f = 2\epsilon_o$ and $\epsilon_f = 4\epsilon_o$, the curves of RCS versus α have a trend opposite to those of the other two profiles. With $\epsilon_f = 2\epsilon_o$ the RCS increases to the maximum around $\alpha = 30°$, and then decreases. With $\epsilon_f = 4\epsilon_o$ the RCS decreases with α.

Figure 6 shows the effects of groove number on the RCS. For the wedge profile with $P = 4$ the RCS first decreases with α until $\alpha = 20°$ then increases to the maximum of 17.09 dB at $\alpha = 45°$. For the same profile with $P = 6$ ($P = 8$) the RCS increases with α to the maximum of 18.22 dB (16.42 dB) around $\alpha = 30°$ ($\alpha = 25°$), and then decreases. The RCS curves of the crack profile have a trend similar to those of the wedge profile. For the cavity profile the RCS curves with $P = 4$ and $P = 6$ have similar shape. The RCS curve with $P = 8$ has a flat region in $15° \leq \alpha \leq 30°$. The maximum RCSs of the crack profile with three different groove numbers are about the same and is the lowest among all three profiles.

Figure 7 shows the RCS at three frequencies ($k_o a = 4\pi$, 2π, and π). At low frequency the RCS of the wedge grooves is larger (smaller) than that of crack (cavity) grooves at all incident angles. At the other

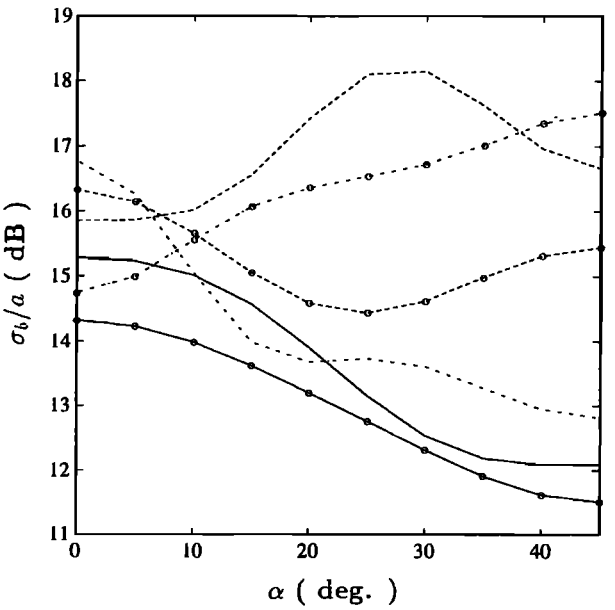

Figure 5. Effects of filling permittivity on the backscattering cross section of a circular cylinder with four grooves, $k_o a = 2\pi$, and $\rho_o = 0.75a$: solid line, cavity profile, $\epsilon_f = \epsilon_o$; dashed line, cavity profile, $\epsilon_f = 2\epsilon_o$; dashed-dotted line, cavity profile, $\epsilon_f = 4\epsilon_o$; solid line with circles, crack profile, $\epsilon_f = \epsilon_o$; dashed line with circles, crack profile, $\epsilon_f = 2\epsilon_o$; dashed-dotted line with circles, crack profile, $\epsilon_f = 4\epsilon_o$.

two frequencies the ranking of RCS with different profiles depends on the incident angle. Intuitively, the backscattering RCS at a high frequency is supposed to be larger than that at a low frequency. However, for the cavity profile the RCS at $k_o a = 2\pi$ is larger than that at $k_o a = 4\pi$ when $12° \leq \alpha \leq 38°$. For the crack profile the RCS at $k_o a = 2\pi$ is larger than that at $k_o a = 4\pi$ when $\alpha \leq 8°$.

4. Conclusions

A mode-matching method has been developed to calculate the radar cross section of perfectly conducting cylinders with arbitrary periodic grooves. Reflection matrices are defined at layer interfaces to reduce the number of unknowns. The effects of profile type (wedge, cavity, and crack), filling permittivity, profile depth, groove number, and frequency on the RCS have been obtained to demonstrate this approach.

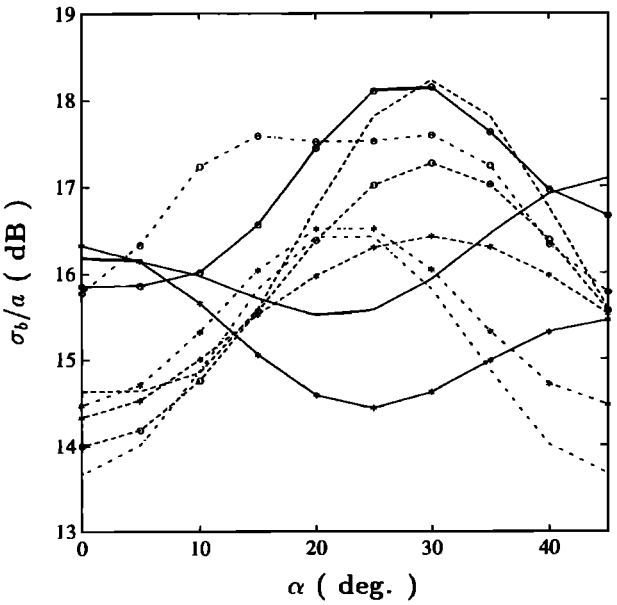

Figure 6. Effects of groove number P on the backscattering cross section of a circular cylinder, $k_o a = 2\pi$, $\rho_o = 0.75a$, and $\epsilon_f = 2\epsilon_o$: solid line, wedge profile, $P = 4$; dashed line, wedge profile, $P = 6$; dashed-dotted line, wedge profile, $P = 8$; solid line with circles, cavity profile, $P = 4$; dashed line with circles, cavity profile, $P = 6$; dashed-dotted line with circles, cavity profile, $P = 8$; solid line with asterisks, crack profile, $P = 4$; dashed line with asterisks, crack profile, $P = 6$; dashed-dotted line with asterisks, crack profile, $P = 8$.

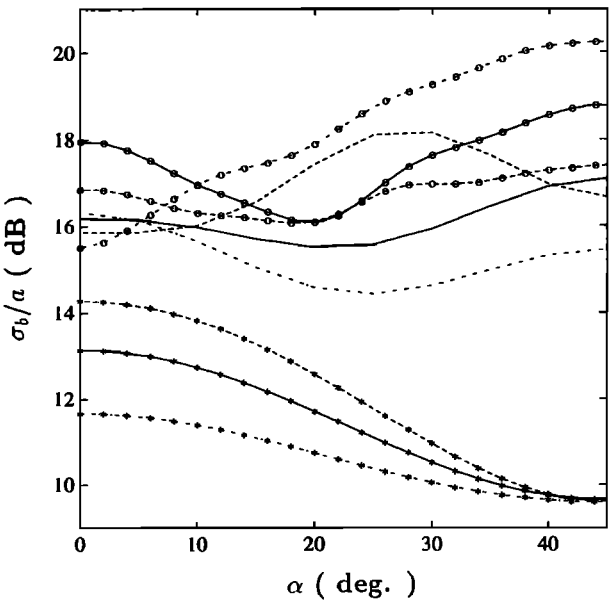

Figure 7. Effects of frequency on the backscattering cross section of a circular cylinder with four grooves, $\rho_o = 0.75a$, and $\epsilon_f = 2\epsilon_o$: solid line with circles, wedge profile, $k_o a = 4\pi$; solid line, wedge profile, $k_o a = 2\pi$; solid line with asterisks, wedge profile, $k_o a = \pi$; dashed line with circles, cavity profile, $k_o a = 4\pi$; dashed line, cavity profile, $k_o a = 2\pi$; dashed line with asterisks, cavity profile, $k_o a = \pi$; dashed-dotted line with circles, crack profile, $k_o a = 4\pi$; dashed-dotted line, crack profile, $k_o a = 2\pi$; dashed-dotted line with asterisks, crack profile, $k_o a = \pi$.

Acknowledgments. The author would like to thank the reviewers for their helpful comments. This work is sponsored by the National Science Council, Taiwan, under contract NSC-86-2221-E005-011 and the Chung-Shan Institute of Science and Technology, Taiwan, under contract CS-86-0210-D005-001.

References

Asvestas, J. S., and R. E. Kleinman, Electromagnetic scattering by indented screens, *IEEE Trans. Antennas Propag.*, *42*, 22-30, 1994.

Boag, A., Y. Leviatan, and A. Boag, Analysis of electromagnetic scattering from doubly periodic nonplanar surfaces using a patch-current model, *IEEE Trans. Antennas Propag.*, *41*, 732-738, 1993.

Cabayan, H. S., and R. C. Murphy, Scattering of electromagnetic waves by rough perfectly con-

ducting circular cylinders, *IEEE Trans. Antennas Propag.*, *21*, 893-895, 1973.

Colak, D., A. I. Nosich, and A. Altintas, Radar cross section study of cylindrical cavity-backed apertures with outer or inner material coating: The case of E-polarization, *IEEE Trans. Antennas Propag.*, *41*, 1551-1559, 1993.

Goggans, P. M., and T. H. Shumpert, A new surface impedance function for the aperture surface of a conducting body with a dielectric-filled cavity, *IEEE Trans. Antennas Propag.*, *39*, 960-967, 1991.

Harrington, R. F., *Time-Harmonic Electromagnetic Fields*, McGraw-Hill, New York, 1993.

Hoppe, D. J., and Y. Rahmat-Samii, Higher order impedance boundary conditions applied to scattering by coated bodies of revolution, *IEEE Trans. Antennas Propag.*, *42*, 1600-1611, 1994.

Jin, J.-M., and J. L. Volakis, Scattering and radiation analysis of three-dimensional cavity arrays via a hybrid finite-element method, *IEEE Trans. Antennas Propag.*, *41*, 1580-1586, 1993.

Kong, J. A., *Electromagnetic Wave Theory*, 2nd ed., John Wiley, New York, 1990.

Peng, S. T., T. Tamir, and H. L. Bertoni, Theory of periodic dielectric waveguides, *IEEE Trans. Microwave Theory Tech.*, *23*, 123-133, 1975.

Ramahi, O. M. and R. Mittra, Finite element solution for a class of unbounded geometries, *IEEE Trans. Antennas Propag.*, *39*, 244-250, 1991.

Rulf, B., Scattering by a class of composite bodies using generalized separation of variables, *IEEE Trans. Antennas Propag.*, *40*, 843-848, 1992.

Sarabandi, K., and F. T. Ulaby, High frequency scattering from corrugated stratified cylinders, *IEEE Trans. Antennas Propag.*, *39*, 512-520, 1991.

Schiavone, G. A., K. O'Neill, and K. D. Paulsen, H-polarized scattering from single and multiple elon gated cavities, *IEEE Trans. Antennas Propag.*, *41*, 1122-1131, 1993.

Zaki, K. A., and A. R. Neureuther, Scattering from a perfectly conducting surface with a sinusoidal height profile: TM polarization, *IEEE Trans. Antennas Propag.*, *19*, 747-751, 1971.

J.-F. Kiang, Department of Electrical Engineering, National Chung-Hsing University, Taichung, Taiwan

(Received November 29, 1996; revised May 12, 1997; accepted May 16, 1997.)